2021 IEEE Energy Conversion Congress and Exposition (ECCE) | 978-1-7281-5135-9/21/$31.00 ©2021 IEEE | DOI: 10.1109/ECCE47101.2021.9595018

Power Switch Open-Circuit Fault-Diagnosis Based on a Shallow Long-Short Term Memory Neural Network: Investigation of an Interleaved Buck Converter for Electrolyzer applications

Rahul Kumar
The University of the South Pacific
Suva, Fiji
rahul.kumar@usp.ac.fj

Shanal Kumar
The University of the South Pacific
Suva, Fiji
s11121467@student.usp.ac.fj

Giansalvo Cirrincione
University of Picardy Jules Verne,
Amiens, France
giansalvo.cirrincione@u-picardie.fr

Maurizio Cirrincione
The University of the South Pacific
Suva, Fiji
maurizio.cirrincione@usp.ac.fj

Damien Guilbert
Université de Lorraine, GREEN, F-54000, Nancy, France
damien.guilbert@univ-lorraine.fr

Krishnil Ram
The University of the South Pacific
Suva, Fiji
ram_k@usp.ac.fj

Ali Mohammadi
The University of the South Pacific
Suva, Fiji
ali.mohammadi@usp.ac.fj

***Abstract*— Hydrogen energy conversion using Fuel Cells is very promising for standalone power as well as transportation applications. Hydrogen gas production using renewable energy sources is possible through the use of electrolyzers in which DC-DC converters play an important role. This paper presents an accurate and robust method of fault diagnosis and condition monitoring applied to an interleaved DC/DC buck converter that supplies a proton exchange membrane (PEM) electrolyzer. This work mainly focuses on power switch open-circuit failures. The study gives excellent results in the early detection of faults to improve the reliability of PEM electrolyzers. A suitable experimental test bench has been realized to obtain data under healthy and faulty operating conditions. A preliminary exploratory analysis of the data has been carried out using a linear approach to understand the geometry of the data and suggest a suitable tool for classifying the system's condition. The paper then proposes a shallow configuration Long Short Term Memory (LSTM) based neural network capable of detecting and localizing the fault at every time step without any pre-processing. The experimental results presented in this paper show that, after a detailed comparison with other 25 neural and non-neural based techniques for classification, the shallow LSTM neural network gives the best results.**

Keywords—neural networks, fuel cell, Interleaved Buck Converter (IBC), diagnostics, power switch open-circuit fault, Long Short Term Memory (LSTM)

I. INTRODUCTION

Fuel Cells provide zero carbon emission with only heat and water as byproducts. Hydrogen is the primary fuel in a Fuel Cell (FC) where it is combined with oxygen to generate electricity. There are several methods of generating hydrogen from different input materials [1]. The generation of hydrogen from renewable energy using the electrolysis process is one of the few hydrogen production processes with very low carbon dioxide emissions [2]. A Proton Exchange Membrane (PEM) electrolyzer works in the opposite way to a PEM Fuel Cell. Distilled water is injected at the electrolyzer's anode powered by energy that allows splitting water into hydrogen and oxygen. The protons go through the membrane to the cathode where hydrogen is generated. Since the PEM electrolyzer should be supplied with a very low DC voltage (around 8 V), a step-down DC-DC converter is required for this application [3]. In DC-DC converters, the most fragile components are electrolytic capacitors and power switches. Power switch open-circuit failures (OCF) and an Interleaved DC-DC Buck Converter (IBC) are studied in this work. Any OCF occurring in the DC-DC converter will affect the electrolyzer's operation [4], [5]. Indeed, in IBCs, power switch OCF increases output current ripple (electrolyzer side) and additional current stresses on the healthy power switches [6]. As demonstrated in the literature, a high current ripple affects the electrolyzer's specific energy consumption, and additional current stresses may lead to power switch failures [7].

In the literature, different power switch fault-diagnosis methods have been developed for IBC [8, 9] particularly for photovoltaic and FC applications. The main fault-diagnosis methods are based on sliding mode observers, and monitoring of the input or output current. However, there is a gap in the literature for electrolyzer applications to enhance the DC-DC converter's reliability supplying a PEM electrolyzer. Artificial Intelligence (AI) approaches have been successfully implemented for fault diagnosis of PEMFCs. In particular, an ANN model of PEMFC to control oxygen ratio in real-time has been developed by Damour et al [10]. In this model, the computational time was very low compared to other non-linear model-based controllers. A further contribution was made by Kumbur et al [11] who have implemented the ANN to design the gas diffusion layer of the FC. In comparison, the combination of the ANN model with fuzzy logic have been presented by Justesen et al. In addition, Silva Sanchez et al used this kind of model for diagnostic of PEMFC [12-13]. Recurrent Neural Networks (RNN) can deal with time sequence data [14] and have been used in fault diagnostics of PEM Fuel Cell applications [15]. LSTM neural networks offer better control over the gradient flow and are designed to avoid long-term dependency problems, so that it is easy to

learn and increase accuracy. LSTM is also a possible way to decrease the number of the sensors to develop the efficiency of the PEMFC [16]. Ma et al [17] implemented the LSTM for degradation prediction of the PEMFC model in long and short periods. The results showed that the LSTM has much accurate results compared with traditional RNN. Fault diagnosis in DC-DC converters can be divided into Model-Free or Model-Based Methods [18]. The proposed strategy does not use a mathematical model of the system and is therefore similar to a data-driven approach, which can update its parameters based on the network's inputs. The idea here is to detect and localize the power switch OCF instantaneously to avoid any permanent failure to the DC-DC converter and the resulting damage to the electrolyzer. The proposed methodology realizes a shallow LSTM neural network, which is very suitable for data already in sequence form. The proposed neural architecture is very simple, and due to its low time complexity, the network can generate classes (healthy, faulty, and location of the fault) quickly. Besides, unlike other neural and non-neural based approaches (25 classifiers are compared in this paper), the proposed shallow LSTM neural network gives probabilities for each class at every time step. This assists in performing subsequent risk analysis.

II. EXPERIMENTAL TEST – FAULT EMULATION

An experimental test rig has been realized at the GREEN laboratory, IUT de Longwy as shown in Fig 1. The experimental test bench is made up of an autotransformer (input), a SEMISTACK IGBT from SEMIKRON Company to realize the 3-phase diode rectifier and the 3-phase IBC (see Fig 2), passive components (inductors and capacitor), and a PEM electrolyzer from HELIOCENTRIS Company supplied by a pure water tank. The technical specifications of the used PEM electrolyzer and the system are provided in Table I. The control of the IBC based on a PI controller has been realized in the Matlab/Simulink environment, and then it has been transferred into a DS1104 dSPACE controller board. Since the PWM gate control signals of the IBC must be shifted from each other by 120°, a microcontroller has been employed for this purpose. To simulate OCFs, a programming code has been implemented into the microcontroller. This code is linked with a push-button switch located outside the controller. When the push button switch is OFF, the PWM gate control signal from dSPACE controller board is sent to the IBC. In comparison, if the push button switch is ON, the PWM gate control signal is set to 0, simulating an OCF. The measured current data of the IBC are acquired by current clamps PAC12 from Chauvin-Arnoux Company (with a probing sensitivity of 10 mV/A) and are saved through the dSPACE Control Desk software.

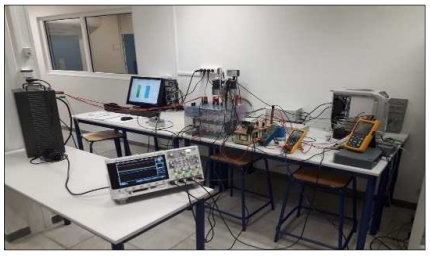

Fig 1. Developed experimental test bench.

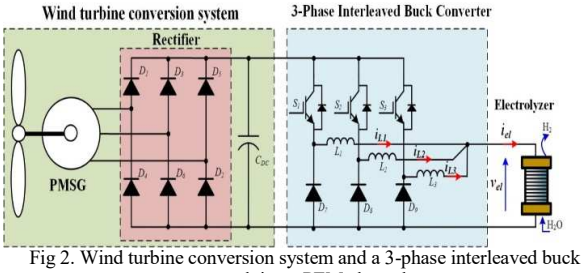

Fig 2. Wind turbine conversion system and a 3-phase interleaved buck converter supplying a PEM electrolyzer.

The data has been acquired by emulating an OCF experimentally on the power switch located in the second and third phases. The obtained results are shown in Fig 3, where the electrolyzer and phase currents of the IBC are depicted. Before the appearance of the OCF (phase 2), it can be observed the current phase ripple. While in phases 1 and 3, the current ripple amplitude is similar; in phase 2 the current ripple is higher due to some deterioration of the inductor. However, this higher amplitude does not affect the obtained results. When generating the OCF in phase 2 (at t=2.25 s), the two remaining healthy power switches compensate the OCF by the increase of the phase current. Since the controller has been designed for a healthy operating mode, an unbalance of current between phases 1 and 3 can be noted. Thus, this unbalance leads to the decrease of the electrolyzer current. In comparison, the current in phase 2 is null, but with the presence of some noise. The measured current signals data is then used for the geometrical study of the data for the purpose of classification using RNNs.

TABLE I. TECHNICAL SPECIFICATIONS OF THE PEM ELECTROLYZER

Parameters	Values
Electrolyzer rated power, P_{el}	400 W
Electrolyzer rated current, I_{el}	50A
Electrolyzer current ripple, Δi_{FC}	<1 A
Operating voltage range V_{el}	7.5-8 V
Inductor, L	400 µH
Capacitor, C	470 µF
Input DC bus voltage, V_{DC}	50 V
Switching frequency, F_s	20kHz
Duty cycle range, D	0.23-0.26

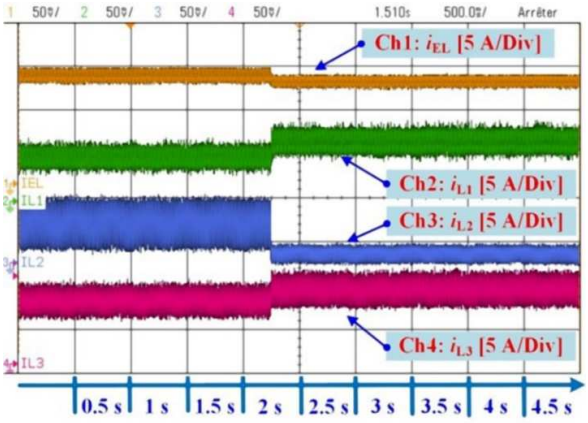

Fig 3. Experimental results (fault in the second phase), time scale: 500ms/div.

III. EXPLORATORY DATA ANALYSIS RESULTS

In order to study the behaviour of the healthy and faulty current signatures, a geometrical analysis with the Principal Component Analysis (PCA) was performed preliminarily [19]. From the Pareto chart (which is derived after applying PCA to the normalized data – Fig. 4a), only four Principal Components (PCs) present the totality of the whole data-set (Note: Pareto charts from faulted Leg 2 and Leg 3 are similar). This quantity is the same as the input to the PCA algorithm. The percentage variabilities of each PC is lower than 30% and are almost similar for all 4 PCs. This distributed variability implies that all the variables (current in all three legs and I_{el}) are necessary.

Moreover, this is also confirmed by the analysis of the principal or canonical angles; indeed, for any pair of flats in a Euclidean space of arbitrary dimension, one can define a set of mutual angles that are invariant under the isometric transformation of Euclidean space. The projected data from PCA has been used and the principal angles have been computed by using the Singular Value Decomposition (SVD) technique. Table II represents the principal angles between healthy and faulty classes, which are illustrated in terms of individual fault progression in legs 2 and 3 and, overall fault progression (both faulted legs). Up to dimensions 1-3, the principal angles were in between $60° - 80°$ while the clusters were nearly orthogonal in dimension 4. This means that regardless of their positions, the healthy and faulty clusters are orthogonal to each other in the 4-D space. However, the two-class clusters appear to be excessively overlapping with each other according to the PCA plots. This complexity is illustrated in Figs. 4b-c, which gives the projection of the data in its first three PCs for faults in Leg 2 and in Leg 3, respectively. Figure 4d shows the projection of the faulted data emanating from both the legs (Leg2 and Leg 3) and demonstrates somewhat the orientation of each class cluster (orthogonality). In both cases (Faults in Leg 2 and Leg 3), the majority of overlap between the healthy and faulty clusters is observed revealing that: linear techniques are not sufficient to explain all the data due to the presence of noise in the data, which makes the problem non-linear. It can be concluded that the separation of the class clusters through linear-based techniques and other standard pattern-recognition approaches will fail. An artificial intelligence approach is explored in the following section.

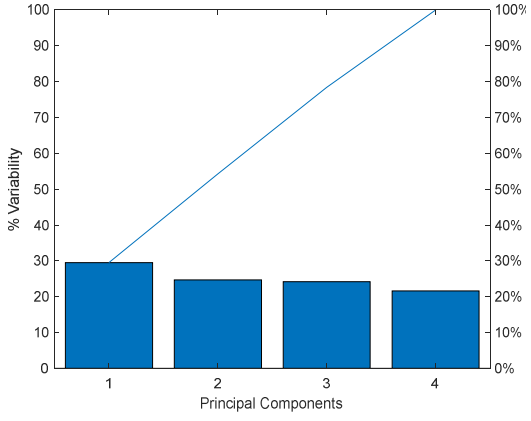

(a)

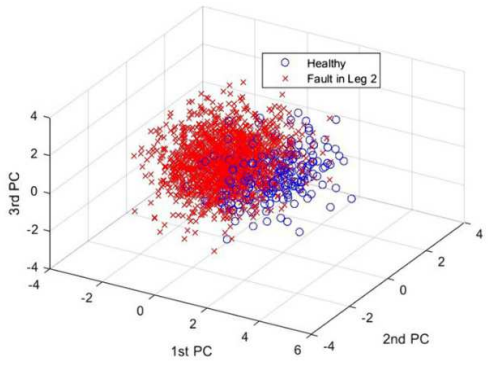

(b)

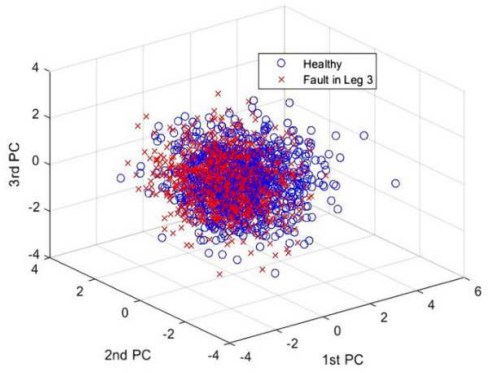

(c)

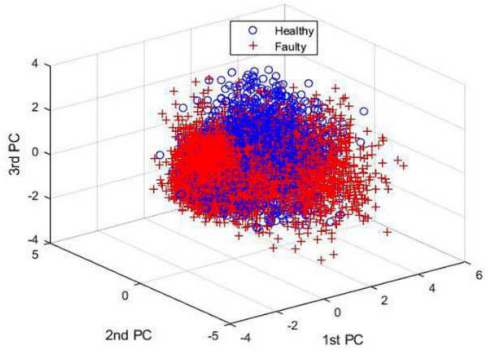

(d)

Fig. 4. (a) Pareto chart for data acquired under leg 2 fault & leg 3 fault (both faulted legs have similar Pareto charts), (b) Principal component plot for data acquired under leg 2 fault, (c) Principal component plot for data acquired under leg 3 fault, (d) Principal component plot for data acquired under leg 2 and 3 faults

TABLE II. PRINCIPAL ANGLES FOR FAULT PROGRESSION IN LEGS 2 AND 3

Dimension (as per PCs)	**Principal Angle - Leg 2** (°)	**Principal Angle - Leg 3** (°)	**Principal Angle - Leg 2& Leg 3** (°)
1	62.12	63.63	62.88
2	71.28	74.50	72.89
3	83.02	81.50	82.26
4	87.41	88.62	88.02

IV. APPLICATION OF SHALLOW LSTM NEURAL NETWORK FOR POWER SWITCH OCF DIAGNOSIS

For online fault detection and localization of time-domain current signals, the RNNs have been instrumental over the past years in the field of deep learning. The LSTM neural network, unlike standard feedforward neural networks, has feedback connections and is able to process not only single data points, but also entire sequences of data. Unlike traditional RNNs, the LSTM was developed to counter the problem of vanishing gradient. A comprehensive description of the LSTM neural network is given in [20].

In this study, a group of neural and non-neural based classification algorithms were trained, validated and tested. To begin with, the raw signals were trained and tested for the classifiers listed in Table III. The training, validation and test sets were randomized and divided into a ratio of 50:10:40 percentages. In the case of neural-based techniques, a window of 20 consecutive 4-D time samples were fed to the network (input tensor of size 1 ×20× 4). Data was augmented by using a stride of 20% of the segment size from one window to the previous one. The total number of sequences as a result of signal segmentation were 754. It should be noted that the window size of 20 samples and mini-batch sizes stated in Table III were chosen after several trials, to obtain the best results in terms of classification accuracy. The results for five neural-based architectures are given in Table III where; the dense/fully connected architectures [21], regardless of being shallow or deep configurations, yielded 64% test accuracy.

V. COMPARISON WITH NON-NEURAL APPROACHES

Similarly, the LSTM based architecture was trained using various combinations of hyper-parameters and the results are presented in Table III. Overall, in terms of neural and non-neural based techniques, the deep configuration of the LSTM neural network gives the highest classification accuracy (**98.34%**) of the test set. On the other hand, the shallow LSTM configuration also has the second-highest test set accuracy, slightly less than the former. Considering the number of trainable parameters, the shallow configuration is definitely superior to the deep LSTM neural network. On this basis and after a thorough comparison with other non-neural based approaches, the shallow LSTM neural network shows the best performance at **97.68%** on the test-set classification accuracy. For the best LSTM architecture, the confusion chart (details about the confusion chart are given in [22]) is shown in Fig. 5, which represents the performance of the classifier on a class basis. The true positives and true negatives are represented diagonally in blue while the others (false positives and false negatives) are represented in a lighter shade. For clarity, Table III accuracy values are normalized and converted into percentages.

For comparison with the non-neural based techniques, a similar data partitioning scheme was adopted and appropriate pre-processing of the input data for each classifier was made. The Tree, Support Vector Machines (SVMs), Discriminant, k Nearest Neighbors (kNNs) and Ensemble based classifiers performed poorly on the raw data despite adopting an optimization criterion for enhancing the system accuracies. Their test accuracies ranged from 38-74% for the 40% test set. It should be noted that the shallow LSTM neural network not only presents the best classifier, but also has the capability to output probabilities without any further calculations. Also, the proposed network not only classifies an oncoming sequence, but gives outputs instantaneously at every time step, as depicted in Fig. 6. It is worth mentioning that the data is labelled in such a way that after a single training, the fault can be detected and simultaneously the location of the fault can be deduced. A clear interpretation of this aspect in real-time is illustrated in Fig. 6.

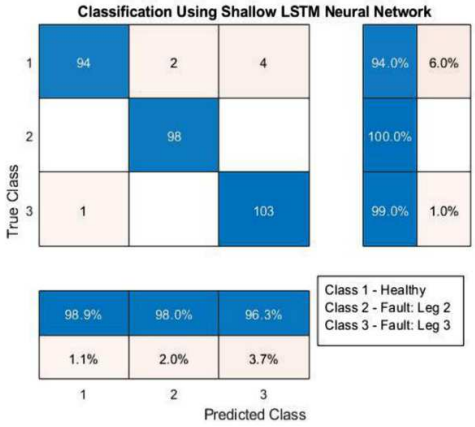

Fig. 5. Confusion Chart for the Shallow LSTM Neural Network

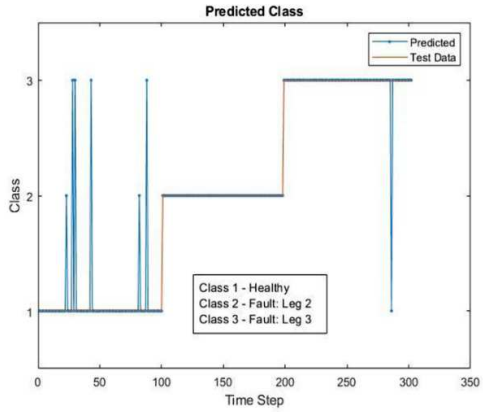

Fig. 6. Prediction using Shallow LSTM Neural Network (includes also classes of faulted legs for fault localization)

VI. CONCLUSION

In this study, an LSTM neural network has been designed to address the problem of power switch OCF in converters, which are usually used for electrolyzer applications. Studying this aspect of the fault when it comes to the protection of electrolyzers is essential. Early detection of faults would help avoid permanent damage to the electrolyzers, avoid degradation of the converters and increase their remaining useful lifetime. The proposed shallow LSTM architecture is able to detect the faulty sequence and deduce in which leg the power switch OCF has occurred. The diagnosis was performed on experimental data, and after training the network, the outputs were generated on a real-time basis. A thorough comparison within several neural based techniques and with non-neural based approaches reveals that the RNN's performances are much superior with low time complexity under the recall phase under this application. The best classification model is a shallow LSTM neural network with 1263 trainable parameters unlike the deeper configuration of LSTM neural network, which had a higher number of

learnable parameters i.e. 313,163. Based on these conclusions, the effectiveness of the developed network presents a classification accuracy of 97.68% on the test set. Future work will involve more in-depth exploratory analysis of the data and include feature calculation steps for comparison with raw data classification. Emerging techniques in Deep Learning will also be applied to the same dataset for comparison.

TABLE III. CLASSIFICATION RESULTS FOR TEST SET

Classifier	Classification Accuracy (%) Test Set	Comments
Shallow LSTM Neural Network	**97.68**	LR = 0.001, Batch size =10, 0% dropout rate, State Activation Function: Hyperbolic Tangent , Gate Activation Function: Sigmoid, Input Weight Initializer: Xavier initializer, Recurrent Weights Initializer: Orthogonal Initialization, Output Layer: softmax Architecture: $(\mathbf{20 \times 4})_{IN}\vert\mathbf{10}_{LSTM_{HU}}\vert\mathbf{3}_{FC}\vert\mathbf{3}_{OUT}$, Total no. Parameters = 1263, HU – Hidden Units
Deep LSTM Neural Network	**98.34**	LR = 0.001, Batch size = 20, 0% dropout rate, State Activation Function: Hyperbolic Tangent , Gate Activation Function: Sigmoid, Input Weight Initializer: Xavier initializer, Recurrent Weights Initializer: Orthogonal Initialization, Output Layer: softmax Architecture: $(\mathbf{20 \times 4})_{IN}\vert\mathbf{10}_{LSTM_{HU}}\vert\mathbf{28}_{FC}\vert\mathbf{28}_{LSTM_{HU}}\vert\mathbf{28}_{FC}\vert\mathbf{3}_{OUT}$, Total no. Parameters = 313,163, HU – Hidden Units
Shallow Dense NN	59.14	LR = 0.001, Batch size = 20, State Activation Function: Hyperbolic Tangent, 20% dropout rate (after 1st fully connected (FC) layer), Output Layer: softmax Architecture: $(\mathbf{20 \times 4})_{IN}\vert\mathbf{68}_{FC}\vert\mathbf{Dropout}_{0.2}\vert\mathbf{3}_{FC}\vert\mathbf{3}_{out}$, Total no. Parameters = 547
Deep Dense NN (TANH Activation)	63.06	LR = 0.001, Batch size = 20, State Activation Function: Hyperbolic Tangent, 20% dropout rate (after every fully connected (FC) layer), Output Layer: softmax Architecture: $(\mathbf{20 \times 4})_{IN}\vert\mathbf{32}_{FC}\vert\mathbf{128}_{FC}\vert\mathbf{32}_{FC}\vert\mathbf{3}_{FC}\vert\mathbf{3}_{OUT}$, No. Parameters = 8611
Deep Dense NN (ReLU Activation)	64.34	LR = 0.001, Batch size = 20, State Activation Function: ReLU, 20% dropout rate (after every fully connected (FC) layer), Output Layer: softmax Architecture: $(\mathbf{20 \times 4})_{IN}\vert\mathbf{32}_{FC}\vert\mathbf{128}_{FC}\vert\mathbf{32}_{FC}\vert\mathbf{3}_{FC}\vert\mathbf{3}_{OUT}$, No. Parameters = 8611
Fine Tree	43.71	Max. Number of Splits = 100, Split Criterion: Gini's Diversity index
Coarse Tree	42.72	Max. Number of Splits = 20, Split Criterion: Gini's Diversity index
Medium Tree	43.71	Max. Number of Splits = 4, Split Criterion: Gini's Diversity index
Linear Discriminant	67.88	Full Covariance Structure
Quadratic Discriminant	67.88	Full Covariance Structure
Linear SVM	74.17	Kernel Function: Linear
Cubic SVM	66.89	Kernel Function: Cubic
Fine Gaussian SVM	38.08	Kernel Function: Gaussian, Kernel Scale: 0.79
Medium Gaussian SVM	38.08	Kernel Function: Gaussian, Kernel Scale: 3.2
Coarse Gaussian SVM	38.08	Kernel Function: Gaussian, Kernel Scale: 13.0
Fine kNN	68.54	k = 1, Distance Metric: Euclidean
Medium kNN	57.95	k = 10, Distance Metric: Euclidean
Coarse kNN	52.98	k = 100, Distance Metric = Euclidean
Cosine kNN	65.23	k = 10, Distance Metric: Cosine
Cubic kNN	59.27	k = 10, Distance Metric: Minkowski
Weighted kNN	61.26	k = 10, Distance Metric: Euclidean Distance weight: squared inverse
Ensemble (Boosted Trees)	57.28	Ensemble Method: AdaBoost, Learner: Decision Tree, Max. Splits: 20, Number of Learners: 30, LR: 0.1
Ensemble (Bagged Trees)	53.64	Ensemble Method: Bagging, Learner: Decision Tree, Number of Learners: 30
Ensemble (Subspace Discriminant)	71.19	Ensemble Method: Subspace, Learner: Discriminant, Number of Learners: 30, Subspace Dimension: 5
Ensemble (Subspace kNN)	62.25	Ensemble Method: Subspace, Learner: Nearest Neighbors, Number of Learners: 30, Subspace Dimension: 5
Ensemble (RUSBoost)	54.64	Ensemble Method: RUSBoost, Max. Splits: 20, Number of Learners: 30, LR: 0.1

REFERENCES

[1] R. S. El-Emam and H. Özcan, "Comprehensive review on the techno-economics of sustainable large-scale clean hydrogen production," Journal of Cleaner Production, vol. 220, pp. 593-609, 2019/05/20/ 2019, doi: https://doi.org/10.1016/j.jclepro.2019.01.309.

[2] S. Shiva Kumar and V. Himabindu, "Hydrogen production by PEM water electrolysis – A review," Materials Science for Energy Technologies, vol. 2, no. 3, pp. 442-454, 2019/12/01/ 2019, doi: https://doi.org/10.1016/j.mset.2019.03.002.

[3] D. Guilbert, S. M. Collura, and A. Scipioni, "DC/DC converter topologies for electrolyzers: State-of-the-art and remaining key issues," International Journal of Hydrogen Energy, vol. 42, no. 38, pp. 23966-23985, 2017/09/21/ 2017, doi: https://doi.org/10.1016/j.ijhydene.2017.07.174.

[4] B. Yao, H. Chen, X. He, Q. Xiao, and X. Kuang, "Reliability and failure analysis of DC/DC converter and case studies," in 2013 International Conference on Quality, Reliability, Risk, Maintenance, and Safety Engineering (QR2MSE), 15-18 July 2013 2013, pp. 1133-1135, doi: 10.1109/QR2MSE.2013.6625766.

[5] G. Cirrincione, M. Cirrincione, D. Guilbert, A. Mohammadi, and V. Randazzo, "Power Switch Open-Circuit Fault Detection in an Interleaved DC/DC Buck Converter for Electrolyzer Applications by Using Curvilinear Component Analysis," in 2018 21st International Conference on Electrical Machines and Systems (ICEMS), 7-10 Oct. 2018 2018, pp. 2221-2225, doi: 10.23919/ICEMS.2018.8549112.

[6] D. Guilbert, D. Sorbera, and G. Vitale, "A stacked interleaved DC-DC buck converter for proton exchange membrane electrolyzer applications: Design and experimental validation," International Journal of Hydrogen Energy, vol. 45, no. 1, pp. 64-79, 2020/01/01/ 2020, doi: https://doi.org/10.1016/j.ijhydene.2019.10.238.

[7] F. d. C. Lopes and E. H. Watanabe, "Experimental and theoretical development of a PEM electrolyzer model applied to energy storage systems," in 2009 Brazilian Power Electronics Conference, 27 Sept.-1 Oct. 2009 2009, pp. 775-782, doi: 10.1109/COBEP.2009.5347619.

[8] M. Shahbazi, M. R. Zolghadri, and S. Ouni, "Fast and simple open-circuit fault detection method for interleaved DC-DC converters," in 2016 7th Power Electronics and Drive Systems Technologies Conference (PEDSTC), 2016: IEEE, pp. 440-445.

[9] S. Zhuo, L. Xu, A. Gaillard, Y. Huangfu, D. Paire, and F. Gao, "Robust open-circuit fault diagnosis of multi-phase floating interleaved DC–DC boost converter based on sliding mode observer," IEEE Transactions on Transportation Electrification, vol. 5, no. 3, pp. 638-649, 2019.

[10] C, Damour, M. Benne, C. Lebreton, J. Deseure, B, Grondin-Perez "Real-time implementation of a neural model-based self-tuning PID strategy for oxygen stoichiometry control in PEM fuel cell", Int. J. Hydrog. Energy 39, 12819–12825. doi:10.1016/j.ijhydene; 2014.06.039.

[11] E.C. Kumbur, K.V. Sharp, M.M. Mench "A design tool for predicting the capillary transport characteristics of fuel cell diffusion media using an artificial neural network", J. Power Sources 176, 191–199. doi:10.1016/j.jpowsour; 2007.10.059.

[12] K.K. Justesen, S.J. Andreasen, H.R. Shaker, M.P. Ehmsen, J. Andersen "Gas composition modeling in a reformed Methanol Fuel Cell system using adaptive Neuro-Fuzzy Inference Systems", Int. J. Hydrog. Energy 38, 10577–10584. doi:10.1016/j.ijhydene; 2013.06.013.

[13] R-E. Silva Sanchez, R. Gouriveau, L. Boulon, S. Jemei, D. Hissel, K. Agbossou, N, Yousfi Steiner "Proton Exchange Membrane Fuel Cell degradation prediction based on Adaptive Neuro Fuzzy Inference Systems", Int. J. Hydrog. Energy 39, 11128–11144; 2014

[14] H. Liu, J. Zhou, Y. Zheng, W. Jiang, and Y. Zhang, "Fault diagnosis of rolling bearings with recurrent neural network-based autoencoders," ISA Transactions, vol. 77, pp. 167-178, 2018/06/01/ 2018, doi: https://doi.org/10.1016/j.isatra.2018.04.005.

[15] Z. Zheng et al., "Brain-inspired computational paradigm dedicated to fault diagnosis of PEM fuel cell stack," International Journal of Hydrogen Energy, vol. 42, no. 8, pp. 5410-5425, 2017/02/23/ 2017, doi: https://doi.org/10.1016/j.ijhydene.2016.11.043.

[16] X. Gu, Z. Hou, and J. Cai, "Data-based flooding fault diagnosis of proton exchange membrane fuel cell systems using LSTM networks," Energy and AI, vol. 4, p. 100056, 2021/06/01/ 2021, doi: https://doi.org/10.1016/j.egyai.2021.100056.

[17] R. Ma, T. Yang, E. Breaz, Z. Li, P. Briois, and F. Gao, "Data-driven proton exchange membrane fuel cell degradation predication through deep learning method," Applied Energy, vol. 231, pp. 102-115, 2018/12/01/ 2018, doi: https://doi.org/10.1016/j.apenergy.2018.09.111.

[18] A. Mohammadi, D. Guilbert, A. Gaillard, D. Bouquain, D. Khaburi, and A. Djerdir, "Faults diagnosis between PEM fuel cell and DC/DC converter using neural networks for automotive applications," in IECON 2013 - 39th Annual Conference of the IEEE Industrial Electronics Society, 10-13 Nov. 2013 2013, pp. 8186-8191, doi: 10.1109/IECON.2013.6700503.

[19] R. R. Kumar, G. Cirrincione, M. Cirrincione, A. Tortella, and M. Andriollo, "Induction Machine Fault Detection and Classification Using Non-Parametric, Statistical-Frequency Features and Shallow Neural Networks," IEEE Transactions on Energy Conversion, pp. 1-1, 2020, doi: 10.1109/TEC.2020.3032532.

[20] S. Hochreiter and J. Schmidhuber, "Long short-term memory," Neural computation, vol. 9, no. 8, pp. 1735-1780, 1997.G. Eason, B. Noble, and I. N. Sneddon, "On certain integrals of Lipschitz-Hankel type involving products of Bessel functions," Phil. Trans. Roy. Soc. London, vol. A247, pp. 529–551, April 1955.

[21] R. R. Kumar, G. Cirrincione, M. Cirrincione, A. Tortella, and M. Andriollo, "A Topological Neural Based Scheme for Classification of Faults in Induction Machines," IEEE Transactions on Industry Applications, pp. 1-1, 2020, doi: 10.1109/TIA.2020.3032944.

[22] C. M. Bishop, *Pattern recognition and machine learning*. springer, 2006.